

Research Paper

Magnetic Positive Positioning: Toward the application in space propulsion

Á. Romero-Calvo^{a,*}, F. Maggi^b, H. Schaub^a^a Department of Aerospace Engineering Sciences, University of Colorado Boulder, 3775 Discovery Drive, 80303, Boulder, CO, United States^b Space Propulsion Laboratory, Department of Aerospace Science and Technology, Politecnico di Milano, Via Giuseppe La Masa, 34, 20156, Milan, Italy

ARTICLE INFO

Keywords:

Magnetic Positive Positioning
 Magnetic liquid sloshing
 Ferrofluids
 Space technology
 Low-gravity

ABSTRACT

The sloshing of liquids in low-gravity entails several technical challenges for spacecraft designers and operators. Those include the generation of significant attitude disturbances, the uncontrolled displacement of the center of mass of the vehicle or the production of gas bubbles, among others. Magnetic fields can be used to induce the reorientation of magnetically susceptible propellants and improve the controllability of a fluid system. Despite being proposed in the early 1960s, this approach remains largely unexplored. This paper provides new insight into the prospects and challenges of using magnetic control of space propellants. Key unanswered theoretical and technical questions are identified, highlighting the importance of developing appropriate analytical tools and fluid-magnetic simulation frameworks. New results associated with the reachability, scaling, long-term thermal and radiation stability, and efficiency of paramagnetic and ferromagnetic propellants are presented. Magnetic settling forces are shown to enhance the stability and speed up the oscillatory response of the liquid, leading to more predictable propellant management systems for different scales and filling ratios. These effects are particularly relevant for ferrofluids, whose enhanced magnetic properties make them excellent candidates for active sloshing control applications in space.

1. Introduction

Propellant sloshing has historically represented a major concern for aerospace engineers due to its capacity to disturb the dynamics of space vehicles. During launch, the uncontrolled movement of liquids may lead to a total or partial mission failure [1]. In microgravity, sloshing is characterized by its highly stochastic nature, which complicates the design of propellant management systems and induces additional spacecraft attitude disturbances [2]. Propellant Management Devices (PMDs) are commonly employed to ensure a gas-free expulsion of propellant, fix the center of mass of the fluid and increase the sloshing frequencies and damping ratios [3,4]. However, they also increment the inert mass of the vehicle and complicate numerical simulations [5].

An interesting alternative to classical PMDs and active settling methods relies in the application of electromagnetic fields to generate a gravity-equivalent force. The use of *dielectrophoresis*, a phenomenon on which an electric force is exerted on dielectric materials, was explored by the US Air Force with suitable propellants in 1963. The study highlights the risk of electrical arcing and the need for large, heavy and noisy power sources [6]. The magnetic equivalent, named *Magnetic Positive Positioning* (MP²), has also been suggested to exploit the inherent properties of paramagnetic, diamagnetic and ferromagnetic liquids. This approach requires inhomogeneous magnetic fields to generate magnetic settling forces [7,8].

MP² devices must deal with the rapid decay of magnetic fields with distance, that limits their applicability to relatively small regions. This difficulty may be compensated by employing highly susceptible liquids, such as ferrofluids. Ferrofluids are colloidal suspensions of magnetic nanoparticles developed in the early 1960s to enhance the controllability of rocket propellants [8]. In spite of their numerous applications on Earth, contributions addressing their original purpose in space are scarce. Terrestrial works have explored the natural frequency shifts due to the magnetic interaction [9], axisymmetric sloshing [10,11], two-layer sloshing [12], liquid swirling [13] or the development of tuned magnetic liquid dampers [14,15]. Low-gravity contributions include the gravity compensation experiments performed by Dodge in 1972, that indirectly addressed the low-gravity sloshing of ferrofluids subjected to quasi-uniform magnetic forces [16]. Motivated by the advent of stronger permanent magnets and high-temperature superconductors, the NASA MAPO experiment validated in 2001 the magnetic positioning of ferrofluid solutions in a series of parabolic flights [7]. Such ferrofluids were selected to approximate the linear magnetization curve of liquid oxygen for different magnetic field intensities. Subsequent publications presented refined numerical models and numerical results of technical relevance [17–25]. The axisymmetric and lateral sloshing of water-based ferrofluids was characterized in microgravity when subjected to an inhomogeneous magnetic field as part of the ESA Drop Your

* Corresponding author.

E-mail address: alvaro.romerocalvo@colorado.edu (Á. Romero-Calvo).

Thesis! 2017 [26–28] and UNOOSA DropTES 2019 [29] campaigns. In order to analyze the free and forced oscillations of magnetic liquids in axisymmetric containers, a quasi-analytical simulation framework was recently developed [30].

In spite of the existence of recent works on MP², the actual space implementation is still distant. This paper outlines key technical challenges associated with the MP² concept, including the need for (i) enhanced modeling capabilities, covering both a rigorous treatment of the magneto-hydrodynamic problem and the effects of magnetically-induced liquid viscosity, (ii) studies addressing the long-term thermal stability of ferrofluids, and (iii) fundamental understanding on the long-term space radiation effects on ferrofluids. It also presents novel analyses of the applicability of magnetic liquids to suppress and control fuel slosh, including (i) a theoretical framework to assess the stability of a magnetic meniscus and representative results for liquid oxygen (LOX), (ii) the effects of the filling ratio on the sloshing modes and frequencies, (iii) new insights into the scaling and optimization of magnetic setups, and (iv) an analysis of the impact of ferrofluids in chemical propulsion systems.

Representative space applications dealing with the magnetic control of space propellants are first presented in Section 2. Section 3 discusses the challenges of this technology, reviews the state of the art on different fields of interest, and offers new results of technical relevance. Finally, Section 4 summarizes the conclusions of the work.

2. Space applications

The ability of controlling the position of susceptible liquids by means of magnetic fields in microgravity leads to several potential space applications. Those include, but are not limited to, mass transfer [31–33], thermomagnetic convection [34,35], or micropropulsion [36,37]. The volume force density that enables these technologies is induced by inhomogeneous magnetic fields on susceptible liquids, and adopts the form

$$f_m = \mu_0 M \nabla H, \tag{1}$$

with μ_0 being the permeability of free space, and M and H denoting the magnetization and magnetic fields, respectively. In addition, the *magnetic normal traction*

$$p_m = \mu_0 \frac{M_n^2}{2} \tag{2}$$

should be considered at the liquid interface, where M_n is the normal magnetization component [38]. The pressure-like term is usually neglected for *natural* liquids, such as LOX. However, it becomes relevant for highly susceptible materials [28]. This section briefly describes three conceptual implementations associated with the magnetic management of liquid propellants in space.

2.1. Passive MP²

Magnetic propellant reorientation represents the first and most intuitive space application. By making use of strategically located magnets or electromagnets, it is possible to either attract (para/ferromagnetism) or repel (diamagnetism) the liquid. For instance, a magnet could be placed at the fuel outlet to hold the propellant and ensure a continuous gas-free supply to the engines, as shown in Fig. 1a. This would replace or reinforce existing surface-tension-based PMDs.

This concept was proposed almost simultaneously by the US Air Force [6] and NASA’s engineer Steve Papell [8] in the early 1960s. After remaining dormant for decades, the advent of high-temperature superconductors motivated a renewed interest in this technology. Most recent works originate from the NASA MAPO experiment [7], that studied the magnetic reorientation of a ferrofluid solution in a parabolic flight. Computational Volume-of-Fluid models were developed on the

basis of the Los Alamos RIPPLE code [39] by assuming (i) linear magnetization, (ii) negligible magnetic pressure, (iii) negligible influence of the magnetized liquid on the magnetic field, and (iv) dipolar magnetic field [17]. Initial works demonstrated the magnetic reorientation concept through numerical simulations [18]. With the aim of generalizing these results, Marchetta and Hochstein subsequently employed the dimensionless parameters [19,20]

$$Bo = \frac{\rho g l^2}{\sigma}, \quad Bo_{mag} = \frac{f_m^{axial} l^2}{\sigma}, \quad \tau = \frac{f_m l^2}{\rho l_t} \tag{3}$$

where Bo is the Bond number, defined as the ratio between inertial and surface tension forces, Bo_{mag} is the magnetic Bond number, which compares the magnetic force with surface tension, and τ is the dimensionless time. ρ is the liquid density, g is the inertial acceleration, l is the characteristic length, σ is the surface tension, and l_t is the height of the tank.

The dimensionless parameters in Eq. (3) are particularly useful for characterizing the *critical Bond number* Bo^* as a function of Bo_{mag} and the tank geometry. Under certain circumstances, the combined action of surface tension and magnetic forces can compensate an adverse inertial acceleration and keep the meniscus stable. The Bo^* number is associated with the value of negative acceleration that destabilizes the surface [40]. It is an important parameter for space applications due to its capacity to establish an upper disturbance limit and drive the design of the liquid management system [2,3]. The dependence of Bo^* with the filling ratio [19], of the reorientation time with Bo_{mag} , and of the critical Bond number with Bo_{mag} were explored for the NASA MAPO tank by Marchetta and coworkers [20,21]. Subsequent models extend the computational setup to non-linearly magnetized materials and complex geometries [25]. 3D ANSYS Fluent-based simulations have also been built by making use of User-Defined Functions [22,23]. Alternatively, the retention of LOX in an accelerating environment has been studied by implementing an additional magnetic energy term in the equilibrium model of Surface Evolver [24]. In all cases, the magnetic field generated by the source is computed or measured as a fixed external input. Then, the magnetic contribution is either implemented as a source term (Eq. (1)) in the momentum balance, or as a magnetic energy term added to the energy balance. In both scenarios, the magnetic and hydrodynamic problems are decoupled.

In spite of the aforementioned works, countless scientific and technological questions still remain unsolved. The stability and reorientation time of spherical, ellipsoidal, and complex tanks have to be explored, and the coupled fluid-magnetic problem needs to be solved to study high-density ferrofluids [41]. Furthermore, full-scale implementations and technological demonstrators have not yet been tested.

2.2. Active MP²

The logical evolution of the previous concept is the active propellant management system represented in Fig. 1b. By making use of a series of electromagnets, the center of mass of the liquid (and hence, of the spacecraft) may be displaced to the most convenient position. That may serve to correct a potential thrust vector misalignment or generate a prescribed torque during a ΔV firing. In addition, electromagnets may also be employed to assist in active fuel flow control [32].

A dedicated feasibility study must be performed in order to identify potential scenarios of application. The existence of an imposed inertial acceleration increases the magnetic control requirements, leads to a larger electromagnet mass and/or current, and restricts the range of application of this technology. Moreover, significant uncertainties should be expected in the estimation and control of the position of the center of mass. One of the key relations to explore is the dependence of Bo^* with Bo_{mag} and the geometry of the system. Such curves naturally lead to the sizing and reachability assessment of the system, as exemplified in Ref. [20] for the NASA MAPO experiment.

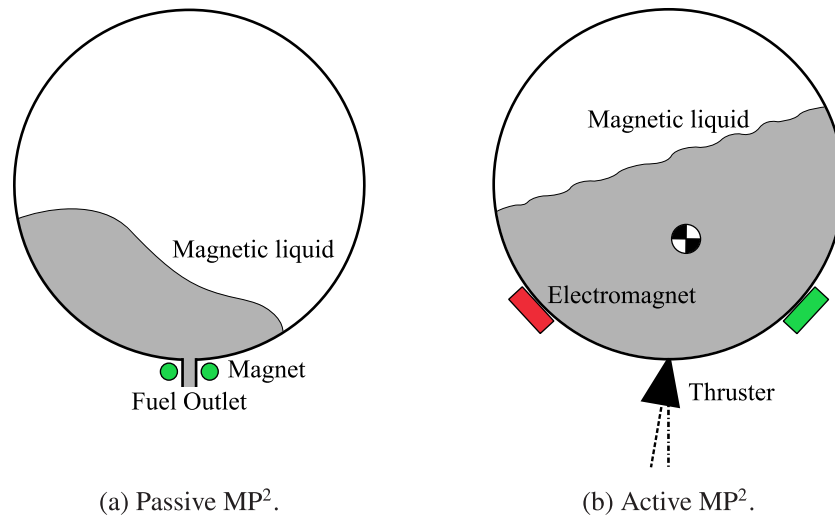


Fig. 1. Conceptual representation of passive and active MP² devices.

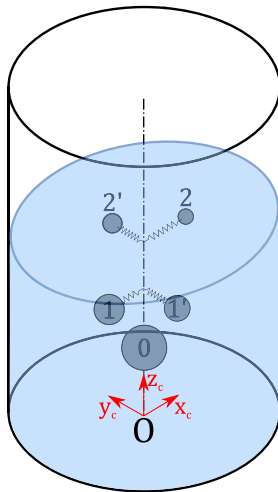


Fig. 2. Modal spring-mass mechanical analogy for inviscid liquid sloshing.

2.3. Magnetic sloshing control

A third concept may seek to develop an overall magnetic sloshing control system. As detailed in Ref. [30], a sufficiently powerful magnetic source would be able to reach a significant portion of the tank volume and modify the response of the liquid to external disturbances. Such force would (i) increase the critical Bond number Bo^* , making the fluid surface less sensitive to external disturbances, (ii) increase the natural sloshing frequencies and damping ratios and, most importantly, (iii) transform a highly stochastic problem into a predictable system. The magnetic liquid sloshing analysis can be performed through numerical simulation [41] or by solving the modal eigenvalue problem that arises from a variational formulation of the inviscid sloshing problem [30]. The second approach follows the track of the classical bibliography on the topic [40,42,43] and leads to fast and computationally efficient predictions of the sloshing dynamics.

Standard mechanical analogies, like the example given in Fig. 2, could be easily embedded into an external controller to predict and compensate the disturbance torque produced by the liquid, improving pointing accuracy and reducing attitude disturbances [30]. As in the previous cases, the study of Bo^* is of paramount importance to size the system.

Table 1

Physical properties of CH₄ (l) enriched with a 0.53% volume of Fe₃O₄ nanoparticles, and of O₂ (l) at cryogenic storage temperature [45–48].

Substance	T [K]	P [bar]	ρ [kg/m ³]	σ [mN/m]	χ_{mi}
CH ₄ (l) + Fe ₃ O ₄ (s)	111	2	448	12.99	Fig. 3
O ₂ (l)	90	2	1141	13.2	0.0042 ^a

^aAccording to Ref. [45], the magnetic susceptibility of liquid oxygen is 0.0042 at 60 K and zero pressure. However, other sources [7,47] employ 0.0034 at 90 K and atmospheric pressure. Since the actual value depends on environmental conditions [45], the first is taken as an upper limit.

3. Scientific and technical challenges

The difficulties associated with the practical implementation of the magnetic propellant control concept in space span from purely physical considerations up to the certification process. This section explores the physical and technical challenges for space systems and the specific difficulties faced by ferrofluid-based propellants.

For illustrative purposes, a LOX/liquid methane (CH₄) in-space bipropellant propulsion system is considered. This combination has been proposed as a green, long-life, and compact enabler for future space exploration with in-situ propellant production [44]. An hypothetical liquid methane ferrofluid with a 0.53% volume concentration of Fe₃O₄ nanoparticles is assumed. This represents a low concentration value in comparison with commercial light-hydrocarbon ferrofluids (~ 18%, Ferrotec EMG-900¹) but still produces a significant magnetic response without compromising the performance of the propulsion system (see Section 3.6).

The physical properties of O₂ (l) and CH₄ (l) + Fe₃O₄ (s) are given in Table 1, with the magnetization curves being represented in Fig. 3. The magnetic behavior of the hypothetical CH₄-based ferrofluid is taken to be equivalent to the 1:10 volume solution of the Ferrotec EMG-700 ferrofluid employed in Ref. [30]. While the increase in density due to the addition of nanoparticles is considered, the surface tension of CH₄ is assumed to remain unaltered.

Propellant and oxidizer are contained in 1U cylindrical tanks with 60 g neodymium magnets surrounding their fuel outlets, as shown in Fig. 4. In the nominal configuration, the contact angle θ_c is 60°, the inertial acceleration g is set to 0 (microgravity), and the magnet is magnetized in the vertical direction at $M_m = 1500$ kA/m. It should be

¹ <https://ferrofluid.ferrotec.com/products/ferrofluid-emg/oil/emg-900/>. Consulted on: 03/07/2021.

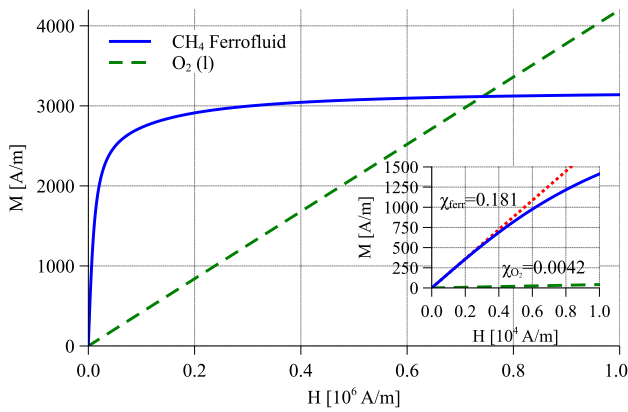


Fig. 3. Magnetization curves of liquid CH₄ enriched with a 0.53% volume of Fe₃O₄ nanoparticles (ferromagnetic) and liquid O₂ (paramagnetic).

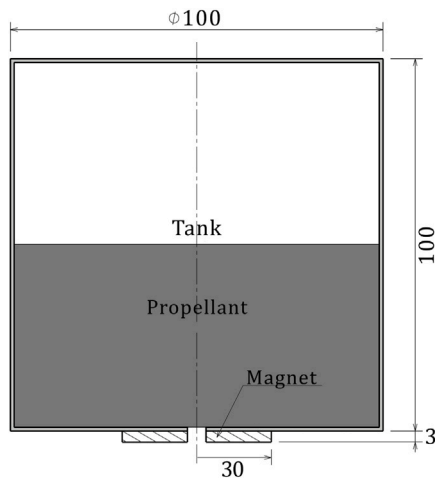


Fig. 4. Sketch of the 1U propellant tank considered in the analysis. Units in mm.

noted that a larger oxygen tank would be employed in actual systems, since the stoichiometric O/F ratio for this configuration is 2. However, the same volume is kept to ease comparison.

3.1. Modeling challenges

The magnetic propellant reorientation concept has been considered an exotic idea until the late 1990s, and theoretical or numerical contributions have been scarce since then. As a consequence, existing modeling capabilities are limited and hardly accessible. In this section, key ways of improvement of existing simulation frameworks are identified. The importance of having a rigorous fluid-magnetic coupling is highlighted.

3.1.1. Numerical simulation

The pioneering contributions by Marchetta and Hochstein made extensive use of numerical models to study the reorientation of magnetic liquids [17–23,25]. However, the authors did not explore the behavior of non-cylindrical tanks and assumed (i) negligible magnetic pressure, (ii) negligible influence of the magnetized liquid position on the magnetic problem, and (iii) constant viscosity coefficients. Although appropriate for natural liquids, these assumptions should be revisited for highly susceptible materials, such as ferrofluids. Their importance can be addressed under different scenarios by means of the fluid-magnetic governing equations. In the fluid problem, the mass and

momentum balances for a magnetic, viscous, and incompressible liquid become [49]

$$\nabla \cdot \mathbf{v} = 0, \tag{4a}$$

$$\rho \frac{D\mathbf{v}}{Dt} = \rho \mathbf{g} + -\nabla p^* + \nabla \cdot \left\{ \eta [\nabla \mathbf{v} + (\nabla \mathbf{v})^T] \right\} + \mu_0 M \nabla H, \tag{4b}$$

with \mathbf{v} denoting the liquid velocity, D the material derivative, p^* the composite pressure (that includes hydrostatic and magnetopolarization terms [38]), η the viscosity coefficient, and t the time. The terms at the right-hand side of Eq. (4b) are, from left to right, the pressure, viscosity, and magnetic contributions of the Maxwell stress tensor. This system of equations is completed with an appropriate set of boundary conditions; in particular, the normal balance at the interface between the magnetic liquid and a non-magnetic, inviscid gas is given by

$$p^* - 2\eta \frac{\partial v_n}{\partial x_n} + p_m - p_0 = 2\sigma H, \tag{5}$$

where \mathbf{n} is the external normal vector, H the mean curvature of the interface, v_n the normal velocity component, and x_n distance along the normal direction. The magnetic pressure term p_m , neglected in virtually all previous works on MP², should be considered for highly susceptible ferrofluids [28].

The magnetic and pressure terms in Eqs. (4b) and (5) are determined by the magnetic, magnetic flux density, and magnetization fields \mathbf{H} , \mathbf{B} , and \mathbf{M} , respectively. For a static magnetic configuration without surface currents and electric fields, those are computed from the steady-state Maxwell equations

$$\nabla \cdot \mathbf{B} = 0, \tag{6a}$$

$$\nabla \times \mathbf{H} = \mathbf{J}_e, \tag{6b}$$

where \mathbf{J}_e is the volume density of electric current and $\mathbf{B} = \mu_0 (\mathbf{H} + \mathbf{M})$. Under the same assumptions, the magnetic boundary conditions are

$$\mathbf{n} \cdot (\mathbf{B}_2 - \mathbf{B}_1) = 0, \tag{7a}$$

$$\mathbf{n} \times (\mathbf{H}_2 - \mathbf{H}_1) = 0, \tag{7b}$$

implying that the normal component of \mathbf{B} and the tangential component of \mathbf{H} are continuous across the liquid–gas interface.

In light of Eqs. (4) and (6), the fluid-magnetic coupling becomes evident: the presence of a magnetizable volume in a magnetic environment modifies the magnetic field \mathbf{H} , and such field drives the momentum balance in Eq. (4b). Neglecting this contribution may lead to significant errors, particularly in microgravity and for highly susceptible liquids. In those cases, the fluid and magnetic problems must be solved simultaneously, as done in Refs. [30] and [41]. Since commercial software suites do not generally implement this capability, it becomes necessary to develop dedicated simulation frameworks.

Past works on MP² focus on natural liquids and implement constant viscosity coefficients. However, applications dealing with concentrated ferrofluids should also consider a magnetically-induced viscosity field. The application of an external magnetic field on ferrofluids aligns the magnetic dipoles with the field lines. Larger velocity gradients appear in their surroundings, increasing viscous dissipation. In other words, the viscosity field of ferrofluids becomes inhomogeneous in the presence of magnetic fields [38]. According to Shliomis [50], the magnetic contribution to viscosity is maximized when the vorticity vector and magnetic field lines are perpendicular, becoming zero if they are parallel. This follows from the relation

$$\frac{\Delta \eta}{\zeta} = \frac{\mu_0 M_0 H \tau}{4\zeta + \mu_0 M_0 H \tau} \sin^2 \beta, \tag{8}$$

where ζ is the vortex viscosity, τ is the Brownian relaxation time, M_0 is the unperturbed magnetization value, and β is the angle between the magnetic field \mathbf{H} and the vorticity vector $\boldsymbol{\Omega}$. For dilute ferrofluids, $\zeta = (3/2)\eta\phi$, with ϕ being the volume fraction of solids [38]. Shen

provides an alternative formulation of this expression for cases with high shear rate under strong magnetic fields [51]. Although an increase in liquid viscosity leads to larger damping ratios and smaller oscillation frequencies, the influence of an inhomogeneous viscosity field on such results still needs to be studied.

3.1.2. Surface stability and critical loads

The classical literature in low-gravity fluid mechanics has devoted significant attention to the stability of liquid interfaces [40]. Space applications make use of the critical Bond number Bo^* , which determines the *critical load* that destabilizes the surface, as a design parameter [2]. Although this problem has been comprehensively studied since the Apollo era, its magnetic equivalent remains practically unexplored. Exceptions are the numerical works by Marchetta and coworkers [18–25] or, more recently, by the authors [41].

Even though the formulation of the magnetic sloshing problem is complicated by the application of highly inhomogeneous force fields, the meniscus stability analysis can still be carried out by means of quasi-analytical tools for relatively simple geometries. Such tools are useful to both fundamental and applied research but, to the best knowledge of the authors, have never been applied to the MP² concept. Referring to Myshkis, *if for a certain position of absolute equilibrium of a liquid the second variation $\delta^2\mathcal{U}$ of the potential energy \mathcal{U} for the mechanical system “liquid + vessel wall” is positive, the position [of the interface] will be stable* [40]. The potential energy \mathcal{U} is expressed as the sum of energies related to the fluid surface S , liquid wall W , gas wall W_g , and mass-force potential Π , which results in

$$\mathcal{U} = \sigma|S| + \bar{\sigma}|W| + \sigma_g|W_g| + \rho \int_V \Pi dV, \tag{9}$$

where $\bar{\sigma}$ and σ_g are the surface tensions of the pairs liquid/wall and gas/wall, respectively, and $|\cdot|$ denotes the area of the corresponding surface. By expressing Eq. (9) in terms of the geometry of the system and computing its second variation, a quadratic functional $\delta^2\mathcal{U}$ is obtained. The application of the principles of calculus of variations to this functional results in an eigenvalue problem that determines the stability of the interface (i.e. a spectral stability criterion). For axisymmetric problems, which are ubiquitous in space technology, it can be split as the sequence of one-dimensional boundary-value problems [40]

$$-\varphi_0'' - \frac{r'}{r}\varphi_0' + a(s)\varphi_0 + \mu = \lambda\varphi_0 \quad (0 \leq s \leq s_1; ' = \frac{d}{ds}), \tag{10a}$$

$$\varphi_0'(s_1) + \chi(s_1)\varphi_0(s_1) = 0, \quad \int_0^{s_1} r\varphi_0(s)ds = 0, \tag{10b}$$

$$-\varphi_n'' - \frac{r'}{r}\varphi_n' + \left[a(s) + \frac{n^2}{r^2} \right] \varphi_n = \lambda\varphi_n \quad (0 \leq s \leq s_1; n = 1, 2, \dots), \tag{11a}$$

$$\varphi_n'(s_1) + \chi(s_1)\varphi_n(s_1) = 0, \tag{11b}$$

with s denoting the arc parameter along the axisymmetric meniscus S that starts at the axis ($s = 0$) and ends at s_1 , μ and λ being unknown parameters,

$$a(s) = \frac{\rho}{\sigma} \left(r' \frac{\partial \Pi}{\partial z} - z' \frac{\partial \Pi}{\partial r} \right) - \frac{z'^2}{r^2} - r''^2 - z''^2 \tag{12}$$

being a function that depends on the radial r and axial z positions and the normal derivative of Π at the interface, and

$$\chi(s_1) = \frac{k \cos \theta_c - \bar{k}}{\sin \theta_c} \tag{13}$$

representing a boundary parameter where θ_c is the contact angle of the liquid with the wall and k and \bar{k} are, respectively, the radial curvatures of the surface S and tank wall W . The functions φ_0 and φ_n are bounded at the origin and denote the axisymmetric and lateral stability modes with increasing eigenvalues λ_{0i} and λ_{1i} for $i \geq 1$. It can be shown that the *critical eigenvalue* is given by

$$\lambda^* = \min\{\lambda_{01}, \lambda_{11}\}, \tag{14}$$

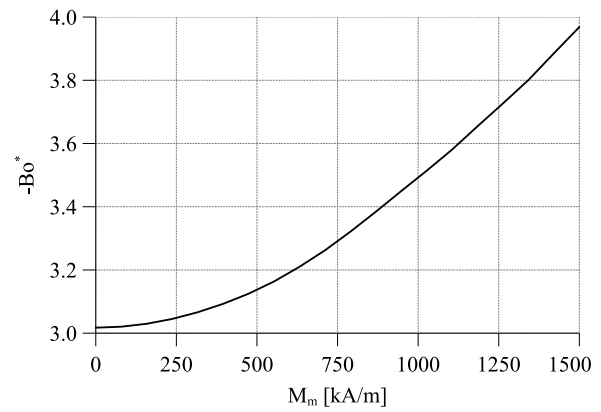


Fig. 5. Dependence of the critical Bond number with the magnetization of the magnet for LOX.

and that the equilibrium state is stable (asymptotically stable, for a viscous liquid) if $\lambda^* > 0$, and unstable if $\lambda^* < 0$ [40]. The nature of the instability is determined by the relative magnitude of the axisymmetric and lateral eigenvalues. For example, if $\lambda_{01} < \lambda_{11}$, the axisymmetric perturbations are *most dangerous*. Alternatively, the stability of the surface can be determined by defining a *critical $\chi^*(s_1)$ parameter*, such that if $\chi(s_1) < \chi^*(s_1)$ the equilibrium state is unstable, and if $\chi(s_1) > \chi^*(s_1)$ it is stable. From the computational perspective, the main advantage of this method is that it substitutes the boundary-value problems in Eqs. (10) and (11) by three second-order ordinary differential equations. Further details can be found in Ref. [40].

The magnetic force in Eq. (1) derives from a potential if the liquid is isothermal [52]. In that case, the mass-force potential Π for inertial and magnetic forces becomes

$$\Pi = gz + \Pi_m, \quad \text{with} \quad \Pi_m = -\frac{\mu_0}{\rho} \int_0^H M(H)dH, \tag{15}$$

which can be readily implemented in the stability analysis through $a(s)$. If a highly susceptible liquid is analyzed, the pressure-like term p_m must be considered in the derivation of Eqs. (10) and (11). For the reasons described in Section 3.1.1, a coupled fluid-magnetic simulation framework must be also employed to solve the liquid interface. Complex geometries or time-dependent problems may instead be studied by means of numerical simulations.

A representative case of application is presented using the geometry in Fig. 4, a liquid height of 5 cm, and LOX. The magnetization of the magnet is increased from 0 to 1500 kA/m and the critical Bond number is computed as the one that makes $\chi(s_1) = \chi^*(s_1)$. The result is plotted in Fig. 5 and shows how Bo^* decreases from -3.017 (which is the non-magnetic value reported in the literature [40]) up to -3.968 , increasing the critical load by a 31.5% with a 60 g magnet.

3.2. Filling ratio dependence

The filling ratio (FR), usually defined as the portion of the total height or volume of the container occupied by the liquid, is a relevant parameter in the computation of the modes and equivalent mechanical analogies of a fluid system [53]. This dependence is complicated by the addition of magnetic sources, that increase the oscillation frequencies and generate a complex meniscus [30]. The accurate modeling of this effect is a key step towards the definition of the operational environment.

Unlike non-magnetic sloshing, a direct generalization of the magnetic results cannot be easily achieved due to the inhomogeneity of the forces involved. In other words, specific configurations have to be analyzed with dedicated simulations. A case of study is here presented for the O₂(l)/CH₄(l) propulsion system described in Section 3. Results

are computed with the coupled quasi-analytical model presented in Ref. [30] assuming the free-edge condition ($\Gamma = 0$). A summary of the theoretical framework is left in the Appendix.

The meniscus profile and magnetic Bond numbers for 40%, 60% and 80% filling ratios are represented in Fig. 6. The small magnetic susceptibility of LOX gives rise to a smooth meniscus profile with limited changes in curvature. In contrast, the combination of low surface tension and high magnetic susceptibility of the methane-based ferrofluid quickly produces a central protrusion. The evolution of the meniscus with the filling ratio is represented in Fig. 7, where the FR=30% level detaches from the lateral wall and has been removed and the FR=100% is shown as a reference without considering the top end of the cylindrical container. It is important to note that the fluid surface tends to follow the constant $B_{o\text{mag}}$ (or H) lines, as reported in the literature [54]. From the physical viewpoint, this is analogous to the tendency of an air balloon to equalize the pressure over its surface. The roles played by air pressure and membrane tension are here assumed by the magnetic force and surface tension, respectively.

An indication of the reachability of the magnet is obtained by analyzing the constant $B_{o\text{mag}} = 1$ lines, that define the transition from magnetic to surface-tension dominated regimes. While for LOX this line crosses the symmetry axis at a height of approximately 64 mm, in the case of the ferrofluid the crossing is produced at $z > 100$ mm due to its enhanced magnetic properties. However, the magnetic Bond number depends on the position and should then be analyzed along the meniscus. This analysis is given in Fig. 8, that illustrates the previous comments and reflects once more the greater susceptibility of the ferrofluid.

Fig. 9 depicts the three first sloshing frequencies for both systems as a function of the filling ratio. As expected, the oscillation frequencies increase when the surface is close to the magnet. While only a slight effect is observed for the O_2 (l) tank (negligible for $FR > 60\%$), increases of the fundamental frequency between a 18% and a 786% with respect to the non-magnetic case are observed for the CH_4 -based ferrofluid.

This analysis shows how ferrofluids may be particularly appropriate for highly demanding magnetic liquid management applications in space, such as active MP² or magnetic sloshing control. Since liquid oxygen has the highest known paramagnetic susceptibility of pure liquids, it is also concluded that non-ferromagnetic liquids may not be well suited for such applications. From the modeling perspective, the strong dependence of the meniscus profile and oscillation frequencies with the filling ratio should be carefully considered in the development of mechanical analogies and the sizing of space systems.

3.3. System scaling

Applications dealing with MP² [7] or magnetic sloshing control [30] work traditionally with either small regions or small propellant tanks due to the rapid decay of magnetic fields. However, an hypothetical design may consider the employment of MP² in larger tanks. The scalability of the system should be then addressed.

In order to illustrate the scaling process, a current loop with radius R and current intensity I is subsequently considered. The magnetic field in the symmetry axis is

$$B_{\text{loop}} = \mu_0 \frac{IR^2}{2(z^2 + R^2)^{3/2}} e_z, \tag{16}$$

where z is the out-of-plane distance and e_z is the unitary vector along the axis. Assuming that magnetization and magnetic fields are collinear and neglecting the surface force component (or, equivalently, assuming a small magnetic susceptibility $\chi \ll 1$), the total force per unit volume induced by the loop on an infinitesimal ferrofluid droplet located in the symmetry axis is

$$F_m \approx \mu_0 M \frac{\partial H}{\partial z} e_z. \tag{17}$$

Making again use of the assumption $\chi \ll 1$, the magnetic flux density due to the magnetization of the ferrofluid can be considered negligible, and hence $B \approx \mu_0 H_0$ inside the drop, with H_0 being the external magnetic field. The internal magnetic field can then be approximated as $H = H_0 - M$. Assuming a linear magnetization curve, where $M = \chi H$, a simplified expression for the total force is obtained as

$$F_m \approx \mu_0 \frac{\chi}{(1 + \chi)^2} H_0 \frac{\partial H_0}{\partial z} e_z. \tag{18}$$

Since $H_0 = B_{\text{loop}}/\mu_0$, the consideration of Eq. (16) in Eq. (18) results in

$$F_m \approx \mu_0 \frac{\chi}{(1 + \chi)^2} \frac{3I^2 R^4 z}{4(R^2 + z^2)^4} e_z. \tag{19}$$

This expression can be applied to axially magnetized cylindrical magnets with magnetization M_m , radius R and height l by employing an equivalent circular loop with the same radius and current intensity $I = M_m l$.

Eq. (19) unveils some important features of the system. The evolution of F_m with z is strongly influenced by R . An increase in the radius of the current loop for constant intensity reduces (increases) the force for small (large) values of z , respectively. Considering a magnet whose mass is conserved with the modification of R , the new equivalent current intensity becomes $I = M_m l_0 R_0^2 / R^2$ and an increase in R reduces the value of F_m for all z . However, the values of F_m outside the symmetry axis benefit from the more homogeneous field generated by wide magnets.

Most importantly, a geometrical scaling of R , l , and z by a factor K multiplies F_m by $1/K$. The scaled ferrofluid meniscus would then be exposed to $1/K$ times the original force. However, since the magnetic Bond number given by Eq. (3) is multiplied by the square of the characteristic length, the $B_{o\text{mag}}$ number of the new system scales with K . In other words, an upscaling of the liquid tank requires relatively smaller magnetic sources to produce an equivalent $B_{o\text{mag}}$ distribution at the interface. Assuming that $B_{o\text{mag}}$ is kept constant, the dimensionless natural frequency Ω in the free surface oscillations problem (Appendix) remains the same, while the dimensional frequency ω evolves with $1/K^3$. This conclusion is exemplified in Fig. 10 after enlarging the nominal CH_4 propellant tank by a factor $K = 10$. The radius of the magnet is then reduced from 30 to 15 cm to approximately recover the original magnetic Bond number distribution, achieving a 75% mass reduction (45 kg for a magnet density of 7100 kg/m³). Including the weight of the magnetic nanoparticles and the magnet, the total mass of the magnetic control system becomes 31 kg, representing a 12% of the propellant mass (282 kg for 80 cm filling height). This value can be significantly reduced with a dedicated optimization process.

As a final remark, Eq. (3) shows that the critical acceleration g^* scales with $1/K^2$ for geometrically similar configurations (i.e. same $B_{o\text{mag}}$). Even if $B_{o\text{mag}}$ scales with K , g^* will decrease more rapidly, and so a careful selection of critical acceleration loads is required for large tanks. Again, this trade-off analysis should be supported by numerical or quasi-analytical models.

3.4. Thermal stability of ferrofluids

Some of the most promising applications of ferrofluids are related to thermal management and space propulsion. These environments may potentially expose the colloid to high temperatures and induce an accelerated agglomeration of the nanoparticles. However, if ferrofluids are sought to be employed in space, their long-term thermal stability must be first guaranteed.

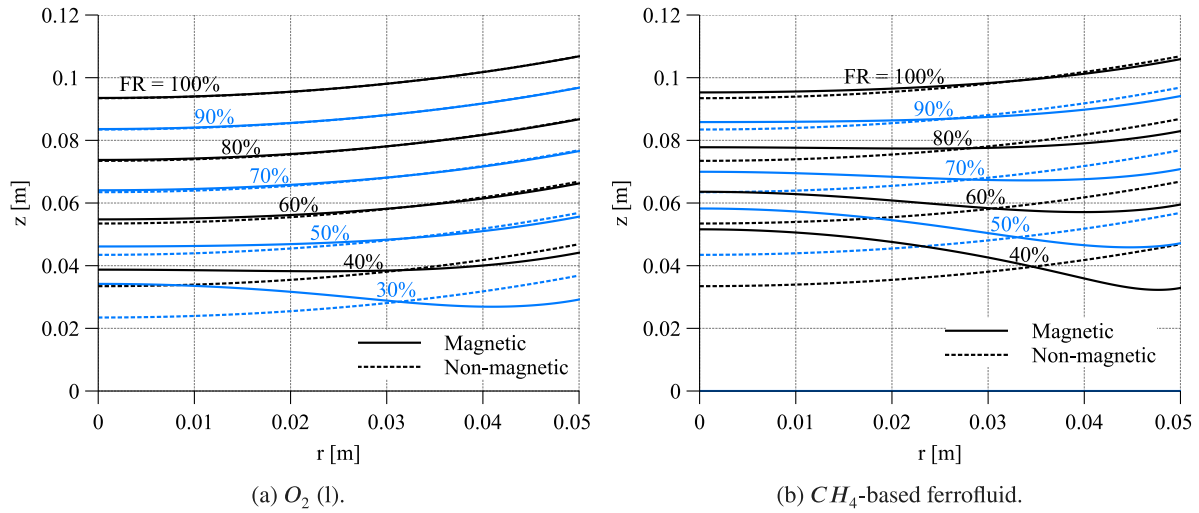


Fig. 7. Axisymmetric meniscus profile as a function of the filling ratio (FR).

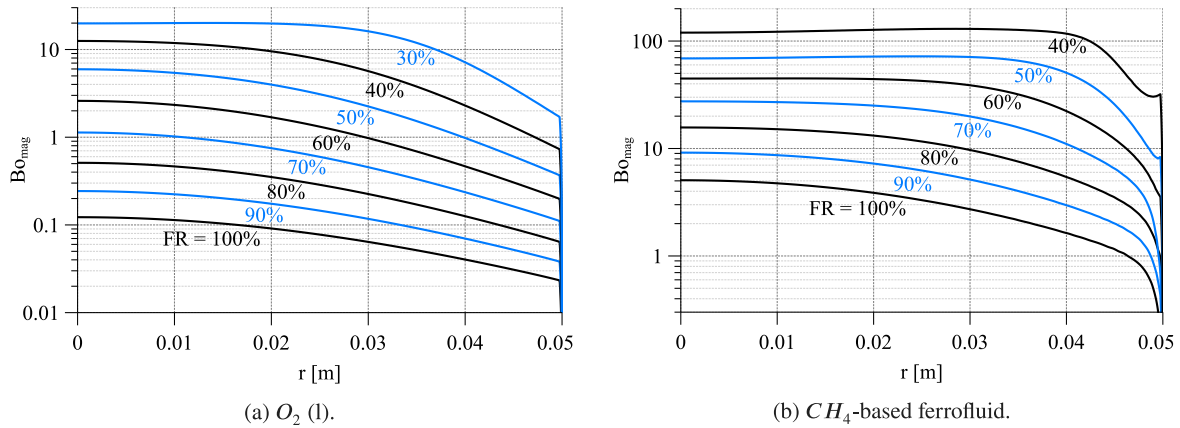


Fig. 8. Magnetic bond number at the axisymmetric meniscus as a function of the filling ratio (FR).

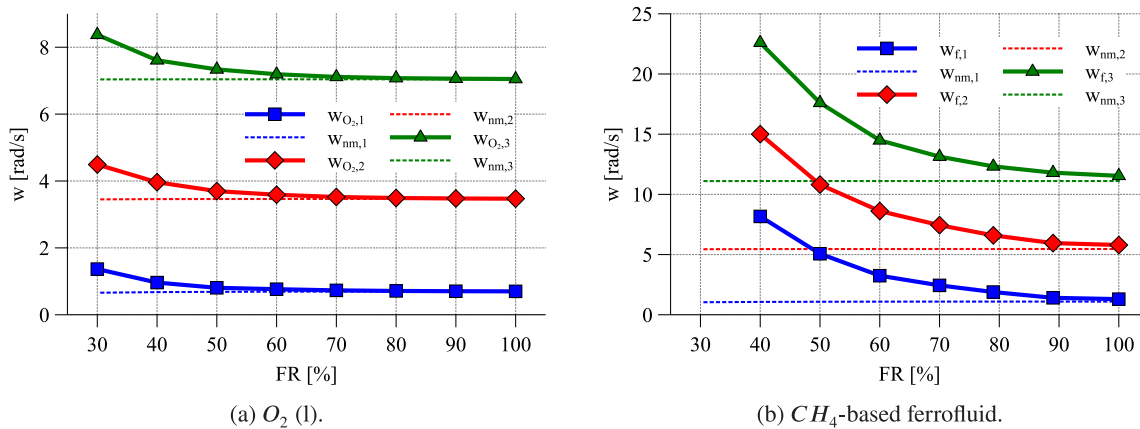


Fig. 9. Fundamental free-edge sloshing frequencies as a function of the filling ratio (FR).

3.4.1. Theoretical framework

The physicochemical stability of a colloid is determined by the balance between the energetic contributions of the system. Under specific environmental conditions, a sufficiently small particle avoids settling (decantation to the sources of potential) and agglomeration (union of several particles) if an appropriate surfactant is employed to overcome the Van der Waals attraction. The excellent discussion on the stability requirements of ferrofluids provided by Rosensweig

in Ref. [38] is summarized in Table 2, where the maximum particle diameter d that overcomes magnetic and gravitational settling, and dipole–dipole agglomeration, is given. In these expressions, $k = 1.38 \cdot 10^{-23}$ J/K is the Boltzman constant, T is the absolute temperature, $\Delta\rho = \rho_{\text{solid}} - \rho_{\text{liquid}}$ is the differential density, L is the elevation in the gravitational field, and $V = \pi d^3/6$ is the volume of the particle.

The dipole–dipole force acts together with the Van der Waals attraction, always present due to the fluctuating electric dipole–dipole forces.

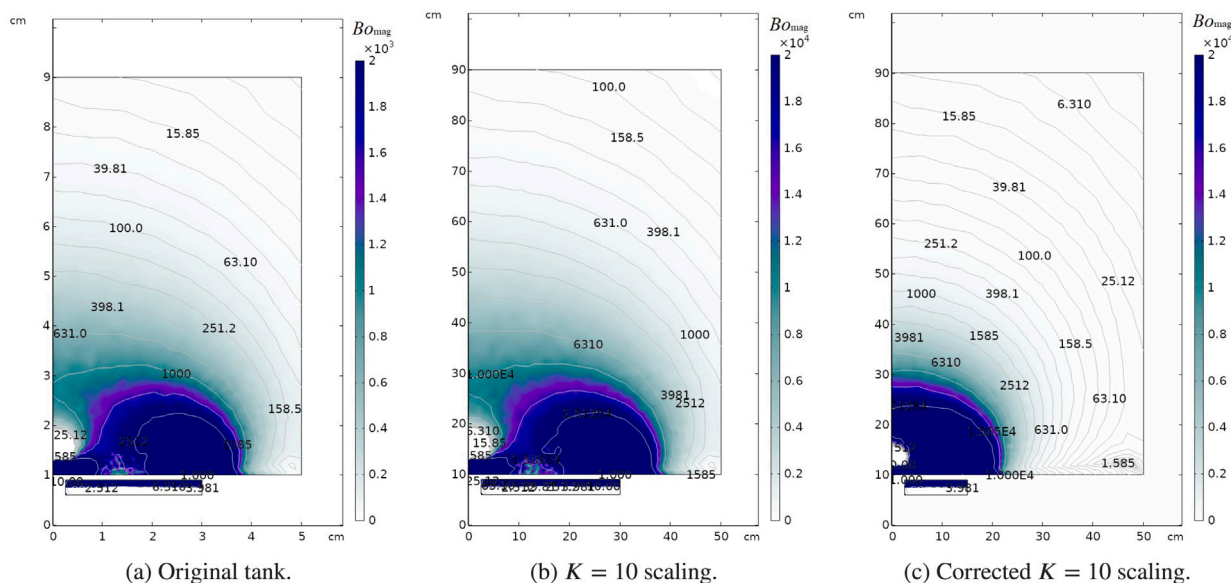


Fig. 10. $B_{o\text{mag}}$ distribution (color scale) in a CH_4 -based ferrofluid with $\text{FR} = 80\%$ and a flat surface. (For interpretation of the references to color in this figure legend, the reader is referred to the web version of this article.)

Table 2

Maximum particle diameter as given by key energy balances.

Symbol	Expression	Comment
d_{max}^m	$\left(\frac{6kT}{\pi\mu_0MH}\right)^{1/3}$	Addresses settling due to magnetic sources
d_{max}^g	$\left(\frac{6kT}{\pi\Delta\rho gL}\right)^{1/3}$	Addresses settling due to gravitational energy
d_{max}^{dd}	$\left(\frac{72kT}{\pi\mu_0M^2}\right)^{1/3}$	Addresses agglomeration due to dipole–dipole interaction

Assuming spherical particles, its associated energy would be

$$E_{V.d.W.} = -\frac{A}{6} \left[\frac{2}{l^2 + 4l} + \frac{2}{(l + 2)^2} + \ln \frac{l^2 + 4l}{(l + 2)^2} \right], \quad (20)$$

with $l = 2s/d$, s being the surface-to-surface separation distance and A the Hamaker constant, approximately equal to 10^{-19} for Fe, Fe_2O_3 , or Fe_3O_4 in hydrocarbon. Unlike the magnetic dipole–dipole energy, Eq. (20) diverges when $s \rightarrow 0$. In other words, the contact between particles must be physically avoided to prevent agglomeration, as thermal energy is unable to prevent coagulation. The problem is commonly solved by adding a surfactant layer made of long chain molecules, producing a mechanism known as steric or entropic repulsion which follows Mackor’s theory [55]. Alternatively, the particles may be charged to generate a Coulomb repulsion, producing ionic ferrofluids. The agglomeration rate is finally determined by the net potential curve, obtained as the difference between attractive and repulsive energies. For very short separation distances the Van der Waals attraction is dominant; otherwise, the steric repulsion prevents the contact. Consequently, two given particles collide only when their thermal energy is greater than the maximum of the net potential. If this energy barrier is well designed (i.e. only a negligible portion of the critical thermal energy distribution overcomes the steric repulsion barrier), the ferrofluid should remain in good condition for long periods of time [38].

3.4.2. Space applications

Space applications dealing with ferrofluids must carefully consider this trade-off analysis. The mission may expose the liquid to (i) launch accelerations of up to $10 g_0$, (ii) long-term microgravity conditions, and (iii) significant thermal gradients. In principle, the first two points represent minor concerns, as the time required to change the equilibrium profile of the colloid is several orders of magnitude larger than the

high-gravity window [56,57] and the process is reversible [38]. On the contrary, colloids subjected to excessive temperatures experience an accelerated thermal aging leading to sedimentation and the degradation of magnetic properties [58].

For the CH_4 -based ferrofluid propellant here considered, $d_{\text{max}}^m = 15 \text{ nm}$, $d_{\text{max}}^g = 3 \text{ nm}$ and $d_{\text{max}}^{dd} = 149 \text{ nm}$ for a storage temperature $T = 111 \text{ K}$, maximum magnetic field $H = 10^5 \text{ A/m}$, maximum magnetization field 2900 A/m , launch acceleration $g = 10g_0 \text{ m/s}^2$, differential density $\Delta\rho = 7450 \text{ kg/m}^3$ and elevation length $L = 0.1 \text{ m}$. The selection of the surfactant is subject to additional requirements (e.g. resistance to low temperatures, space radiation or compatibility with the carrier liquid) and falls beyond the scope of this preliminary analysis. It should be noted that launch accelerations lasts for few minutes and that the condition $d < d_{\text{max}}^g$ may hence be relaxed. This is further supported by the correct execution of past ferrofluids experiments at the ISS [33].

3.5. Radiation stability of ferrofluids

Long-term exposure to space radiation may also degrade the ferrofluid solution and modify its magnetic response. The literature addressing this problem is scarce, focusing mainly on biomedical applications, and can be hardly extended to the space environment due to methodological and application-related issues.

3.5.1. State of the art

Early studies by Kopčanský et al. report strong reductions in the initial susceptibility (13%–40%), saturation magnetization (6%–25%) and magnetic particles concentration (10%–36%) of a stabilized kerosene-based ferrofluid after being exposed to 4.5–17.3 Gy of ^{60}Co γ -radiation with a dose rate of $1.3 \mu\text{Gy/s}$. This degradation is attributed to the destruction of the long polar chain molecules composing the surfactant. Similar experiments on a non-stabilized Fe_3O_4 diester-based ferrofluid show equivalent reductions of the saturation magnetization and a strong influence in the stabilization process [59]. Bădescu et al. also report reductions in initial susceptibility and saturation magnetization of a 5%–10% in kerosene-based ferrofluid subjected to 5–20 Gy of γ -radiation. The same effect is not observed for water-based solutions, attributing this behavior to the superficial anisotropy produced by the implantation of free oleic acid molecules on the particle surface [60]. Recent works with Gd_2O_3 -based ferrofluids using CTAB as a surfactant and ethanol as a carrier liquid analyze the development of intragranular

defects due to γ -ray radiation doses between 32 Gy and 2635 kGy. Results suggest the existence of a critical dose beyond which the defects tend to saturate [61]. The same research group explored the effects of 878 Gy and 2635 kGy γ -radiation doses on the particle size and size distribution dependent spectroscopic and magneto-optic properties of a water-based Fe_3O_4 ferrofluid solution, finding a clear particle distribution dependence, among other results that fall beyond the scope of this work [62].

The effects of electron irradiation on biocompatible water-based ferrofluids are explored by Tomašovičová et al. with sodium oleate and double layer sodium oleate/PEG surfactants [63]. Stable reductions in saturation magnetization of a 50% and a 25% are respectively measured after applying an irradiation dose of 1000 Gy, although most of the loss is already produced for 5 Gy. PEG is shown to behave as a protective surfactant against radiation, with this capability being independent of its molar weight [64]. The degradation process is attributed to the aggregation of particles produced by ionization. Similar experiments with bovine serum albumin (BSA) modified ferrofluids containing sodium oleate stabilized Fe_3O_4 nanoparticles show a dependence between the BSA/ Fe_3O_4 w/w ratio and the stability against radiation [65].

Studies with a technical scope have also been presented. Ferrofluid feedthrough (FF) rotary seals are exposed in Ref. [66] to a mixed radiation environment consisting of fast neutrons (0.2 MGy), protons (2 MGy) and γ -rays (20 MGy). Serious magneto-viscous damages are reported for radiation levels above 2 MGy. Ref. [67] reports the negative impact of a 900 MHz 30 W electromagnetic radiation on the discharging current of transformer oil ITO 100. As a last example, in Ref. [68] microwave heating applied during the synthesis of aqueous ferrofluids is shown to increase the saturation magnetization and have a negligible effect on the stability properties.

3.5.2. Space environment effects

From the material sciences perspective, none of the previous works can be easily extended to the space environment. This is due to the fact that (i) the space radiation dose is small (of the order of 0.4 Gy/year for the ISS orbit, and 1.2 Gy for a 3-years Mars mission), (ii) the tests are performed with radiation sources whose spectrum differs significantly from the space environment (^{60}Co), and (iii) different types of nanoparticles, coatings, and carrier liquids experience different effects. However, a significant degradation for radiation doses below 5 Gy is observed in some of the previous works, so mid-to-long-term effect on ferrofluids should be expected.

Due to the complete lack of space-oriented studies, further experimental efforts are required to estimate the lifetime of a given solution. Future works should address this problem by making use of either high-energy Earth facilities or long-term flight experiments.

3.6. Impact of ferrofluid-enriched propellants on the propulsion subsystem

Slurry fuels is a wide class of liquids consisting of a solid phase in the shape of particles, from the submicrometric to some hundreds of micron, suspended in a fluid medium. The use of metal-based particles in liquid propellants has been analyzed since the 1950s with the perspective to enhance ideal propulsion performance [69]. The stabilization of the suspension can be obtained through liquid gelification, treatment with surfactants, use of dispersants, etc. Proposed applications considered different fields of propulsion (from rocket to air breathing) to obtain lighter and more compact systems. Specific impulse and propellant average density augmentation could be obtained, depending on the peculiar properties of the suspended material. As an example, mixtures of aluminum suspended in gelled kerosene, burned in combination with liquid oxygen, were targeted by NASA. Palaszewsky and Zakany described the experience on aluminum suspensions in kerosene, showing theoretical and experimental results up to metal loads of 55% [70]. In the reported case, gelification of the

suspending medium was necessary to stabilize the dispersion. Known issues connected to the use of metal-based slurry fuels are deposition on nozzle and walls, erosion of injectors, and agglomeration of particles during the combustion process. Lifetime of the slurry became a critical aspect for the real application.

Ferrofluids have been associated with space propulsion since their invention. In 1963 Papell already described colloidal suspensions of magnetite on heptane or JP_4 carriers [8]. Water-based ferrofluids may also find application in propulsion systems employing water, like the one described in Ref. [71]. Light hydrocarbons are widely employed as carriers in commercial ferrofluids [38]; however, liquid propellant rocket fuels never made use of iron oxide. Iron-based compounds have been used in the past for soot reduction in the combustion of complex hydrocarbons (e.g. diesel, kerosene), finding experimental confirmation of enhanced catalytic effect when nanometric oxide particles are involved in the reaction [72].

There are different forms of iron oxide and catalytic/decomposition properties depend on the exact molecule. Hematite is the most stable, and its stability depends on reaction temperature and atmosphere. The reduction in a methane environment of Fe_2O_3 has been documented by Ghosh and co-authors between 1073 K and 1298 K. An active role is attributed to the molecular hydrogen generated by the decomposition of the CH_4 molecule [73]. This property has been used in chemical looping combustion processes. As an example, in a paper by Monazam an iron-based compound acts as oxygen carrier between a section of the reactor where Fe_2O_3 oxidizes a fuel and another part where air oxidizes the resulting metal-based material back to hematite. Reportedly, reaction with methane can generate Fe_3O_4 , FeO , or Fe depending on the degree of hematite reduction [74]. Out of the iron oxide family, magnetite (Fe_3O_4) is a combination of the two oxidation states Fe(II) and Fe(III). It is an amphoteric compound arranged in mixed octahedral/tetrahedral configuration (inverse spinel). It is featured by ferromagnetic properties and high electric conductivity [75]. For this reason, magnetite is a perfect candidate for ferrofluids.

From the rocket propulsion viewpoint, iron oxide is a component characterized by low energy content due to its low formation enthalpy. Thermodynamic computations obtained from NASA's CEA [76] are reported in Fig. 11. The specific impulse is computed for the oxidizer-to-fuel ratio of 4 at 20 bar, nozzle pressure ratio of 20 with optimal discharge and frozen expansion model. Chemical equilibrium is assumed in the combustion chamber only. The evaluations are performed at the reference iron oxide content of 1% and 10% and are compared against a baseline without the oxide additive. As expected, the specific impulse decreases constantly once the iron oxide is introduced. The decrement is less than 1% when Fe_3O_4 fraction is 1% and becomes about 5% for the 10% additive mass concentration. The variation is attributed to the reduction of the flame temperature and the increasing value of the molar mass of the mixture [77]. Fig. 11 reports also the average density of the liquid propellant before combustion. Data are considered for liquid propellants at their respective boiling points. This figure of merit concurs to the definition of the volumetric specific impulse (the product between the specific impulse and the propellant average density) and becomes important to rate the compactness of a propulsion system [78]. A 1% addition of magnetite generates +1% density, and 10% additive content leads to +10% density. This trend attributes a global increase to the volumetric specific impulse, showing that the use of ferrofluid dispersed into the propellant can be beneficial from the compactness viewpoint.

4. Conclusions

In this paper, potential MP^2 space propulsion applications are introduced together with their associated technical challenges. Previous contributions are reviewed starting with the formulation of the concept in the early 1960s, and fundamental gaps of knowledge are identified.

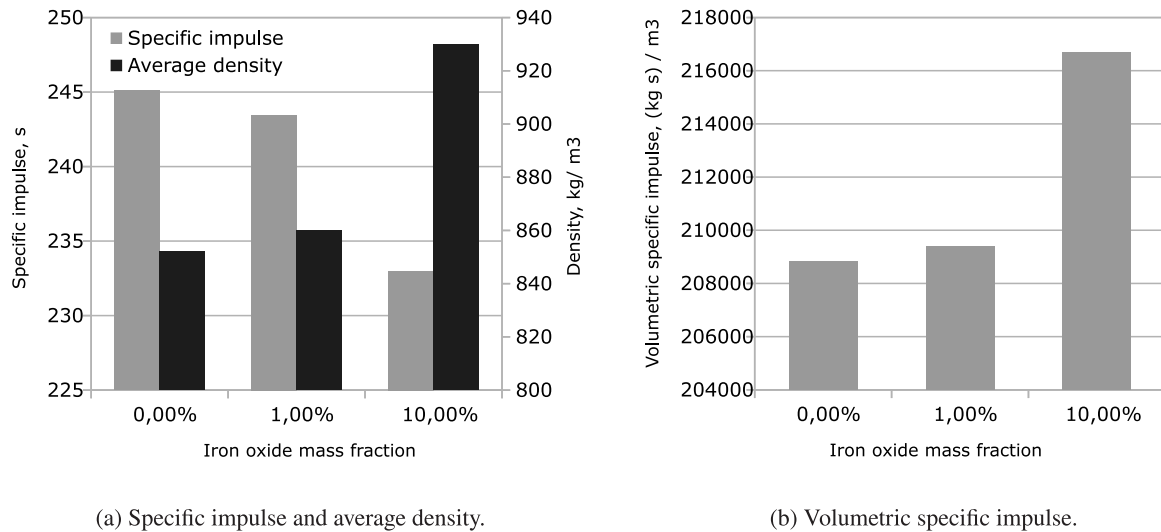


Fig. 11. Analysis of the combustion of $LCH_4/LOX/Fe_3O_4$.

Simulations with LOX and an hypothetical CH_4 -based ferrofluid reveal the strengths and weaknesses of this technology. Due to their small magnetic susceptibility, paramagnetic liquids seem to be limited to low-demanding tasks, such as passive MP^2 . On the contrary, ferrofluids may be employed on active MP^2 and magnetic sloshing control applications. In both cases, the magnetic force is shown to (i) enhance the stability properties, and (ii) increase the natural frequencies of the system. A geometric scaling analysis shows that larger tanks require relatively smaller magnetic sources to induce a similar Bo_{mag} distribution at the interface, but that the critical acceleration decreases proportionally. Careful trade-off studies must be carried out to satisfy the stability and propellant behavior requirements of specific space missions with minimum mass penalties. In this context, the tank filling ratio is shown to have a large effect in the sloshing dynamics of the magnetic liquid.

The technical challenges associated with the employment of ferrofluid-based space propellants are also explored. The need for coupled fluid-magnetic numerical simulation frameworks and inhomogeneous viscosity field modeling is highlighted. Particular attention is devoted to the stability of such solutions against thermal and radiation-induced aging. Although of fundamental importance, the effects of space radiation on ferrofluids seem to be completely unexplored. Finally, it is shown how the addition of Fe_2O_3 nanoparticles to the combustion of O_2 and CH_4 produces a slight decrease of specific impulse and an increase of volumetric specific impulse. This can be beneficial from the propulsion system compactness viewpoint.

Declaration of competing interest

The authors declare that they have no known competing financial interests or personal relationships that could have appeared to influence the work reported in this paper.

Acknowledgments

The authors thank Dr Gabriel Cano-Gómez for his academic assistance, and Dr Daniel Kubitschek for contributing to the initial discussions that motivated this manuscript. The financial support from La Caixa Foundation is gratefully acknowledged.

Funding sources

The project leading to these results has received funding from La Caixa Foundation, Spain (ID 100010434), under agreement LCF/BQ/AA18/11680099.

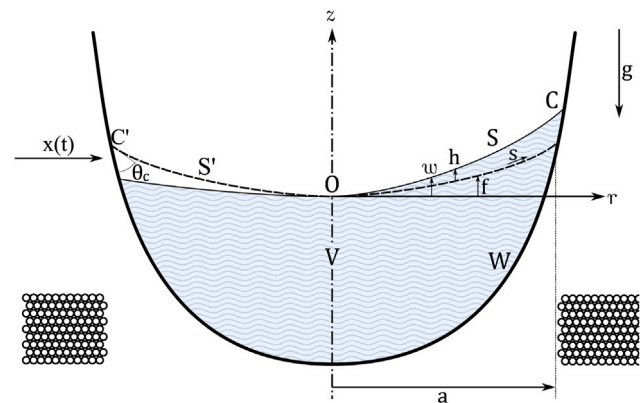


Fig. 12. Geometry of the system. S' refers to the fluid surface, S is the equilibrium meniscus, O denotes the vertex of the equilibrium surface, C is the fluid surface contour, W is the wall of the vessel, and V is the fluid volume [30].

Appendix. Magnetic sloshing model

The magnetic sloshing model presented in Ref. [30] is here summarized. This theoretical framework is assumed in Section 3 to compute the meniscus profile and liquid sloshing modes, and has been shown to provide accurate results for the lateral sloshing measurements of the UNOOSA DropTES 2019 StELIUM experiment [29].

As represented in Fig. 12, in the system under analysis a volume V of magnetic liquid fills an axisymmetric container and develops a meniscus with contour radius a in microgravity. The liquid is incompressible, Newtonian, with density ρ , kinematic viscosity ν , surface tension σ , and wall contact angle θ_c . An applied inhomogeneous axisymmetric magnetic field is imposed by a magnetic source located at the base of the vessel and interacts with the fluid with magnetization $M(H)$. H and M are the modules of the collinear magnetic H and magnetization M fields, respectively. A non-reactive gas with pressure p_g fills the free space. In the figure, s is a curvilinear coordinate along the meniscus with origin in the vertex O and the relative heights are w (fluid surface — vertex), f (meniscus — vertex) and h (fluid surface — meniscus).

A.1. Magnetic meniscus profile

The axisymmetric meniscus profile can be determined from the balance of vertical forces in a segment of the surface [3] or from

the Young–Laplace equation [40], resulting in the set of dimensionless differential equations [30]

$$\frac{d}{dS} \left(R \frac{dF}{dS} \right) = R \frac{dR}{dS} \left[\lambda + BoF - \bar{\psi}(R) \right], \tag{21a}$$

$$\frac{dF}{dS} \frac{d^2 F}{dS^2} + \frac{dR}{dS} \frac{d^2 R}{dS^2} = 0, \tag{21b}$$

and boundary conditions

$$R(0) = F(0) = \frac{dF(0)}{dS} = 0, \quad \frac{dR(0)}{dS} = 1, \tag{21c}$$

$$\frac{dF(1)}{dR} = \tan \left(\frac{\pi}{2} - \theta_c \right), \tag{21d}$$

where $R = r/a$, $S = s/a$, $F = f/a$, $\lambda = a(p_g - p_0)/\sigma$, p_0 is the liquid pressure at the free surface vertex, and $\bar{\psi}$ includes the magnetic terms through

$$\bar{\psi}(R) = \frac{a\mu_0}{\sigma} \left[\int_{H(0,0)}^{H(R,F(R))} M(H)dH + \frac{M_n^2}{2} \right]_{F(R)}, \tag{22}$$

with $\mu_0 = 4\pi \cdot 10^{-7}$ N/A² being the permeability of free space. Although this can be treated as any other boundary-value problem, an iterative shooting method is instead implemented for robustness. Starting from an initial λ value, the system is solved by (i) defining an initial vertex position, (ii) computing the value of λ iteratively in order to satisfy the contact angle condition given by Eq. (21d), (iii) solving the system with an ODE solver, (iv) applying volume conservation to obtain the new height of the vertex, and (v) recomputing the fields H and M with the new geometry. The procedure is repeated until the surface converges with the desired accuracy.

A.2. Modal analysis

The obtention of the magnetic sloshing modes assumes an inviscid, potential, isothermal, and magnetically diluted flow. The free surface eigenfrequencies and eigenmodes can be then computed after linearizing around the meniscus by solving the variational principle

$$\begin{aligned} I &= \iint_{S'} \left[\frac{\mathcal{H}_R^2}{(1 + F_R^2)^{3/2}} + \frac{1}{R^2} \frac{\mathcal{H}_\theta^2}{(1 + F_R^2)^{1/2}} \right. \\ &\quad \left. + (Bo + Bo_{\text{mag}}(R)) \mathcal{H}^2 - \Omega^2 \Phi \mathcal{H} \right] R dR d\theta \\ &\quad - \Omega^2 \iint_W \Phi G R dR d\theta - \Gamma \int_{C'} \left[\frac{\mathcal{H}^2}{(1 + F_R^2)^{3/2}} \right]_{R=1} d\theta \\ &= \text{extremum}, \end{aligned} \tag{23a}$$

subjected to

$$\nabla^2 \Phi = 0 \text{ in } V, \tag{23b}$$

$$\mathcal{H} = \Phi_Z - F_R \Phi_R \text{ on } S', \tag{23c}$$

$$G = \Phi_Z - W_R \Phi_R \text{ on } W, \tag{23d}$$

$$\mathcal{H}_R = \Gamma \mathcal{H} \text{ on } C', \tag{23e}$$

where the subindices denote the partial derivatives and the magnetic Bond number is calculated as

$$Bo_{\text{mag}}(R) = -\frac{\mu_0 a^2}{\sigma} \left(M \frac{\partial H}{\partial z} + M_n \frac{\partial M_n}{\partial z} \right)_{F(R)}. \tag{24}$$

The dimensionless variables $R = r/a$, $Z = z/a$, $F = f/a$, $\phi(R, \theta, Z, t) = \sqrt{g_0 a^3} \Phi(R, \theta, Z) \sin(\omega t)$, $h(R, \theta, t) = \sqrt{a g_0 / \omega^2} \mathcal{H}(R, \theta) \cos(\omega t)$, $\Omega^2 = \rho a^3 \omega^2 / \sigma$, and $\Gamma = a\gamma$ are employed with g_0 being the acceleration of gravity at ground level, ϕ the perturbed velocity potential, ω the circular frequency, γ the hysteresis condition parameter, and $\{r, \theta, z\}$ a

set of cylindrical coordinates with center in the vertex of the meniscus. The *free-edge* condition is characterized by $\gamma = 0$, while the *stuck-edge* condition is associated with $\gamma \rightarrow \infty$. G accounts for the non-penetration wall boundary condition.

Once the axisymmetric meniscus S' , defined by the curve $F(R)$, is determined, the system described by Eq. (23) can be solved to obtain the modal frequencies and shapes with Ritz’s method. The reader is referred to Ref. [30] for further details on the solution procedure. Alternatively, the problem may be solved numerically [79].

References

- [1] M. Eswaran, U.K. Saha, Sloshing of liquids in partially filled tanks - a review of experimental investigations, *Ocean Syst. Eng.* 1 (2) (2011) <http://dx.doi.org/10.12989/ose.2011.1.2.131>.
- [2] W.C. Reynolds, H.M. Satterlee, Ch. 11 - liquid propellant behavior at low and zero g, in: *The Dynamic Behavior of Liquids in Moving Containers*, NASA SP-106, 1966, pp. 387–440.
- [3] F. Dodge, *The New Dynamic Behavior of Liquids in Moving Containers*, Southwest Research Institute, 2000.
- [4] S.H. Collicott, E.A. Beckman, P. Srikanth, Conformal tanks: Small-sat propellant management technology, 2019, <https://doi.org/10.2514/6.2019-3874>.
- [5] A.Y. Lee, J. Stupik, In-flight characterization of the Cassini spacecraft propellant slosh modes, *J. Spacecr. Rockets* 54 (2) (2017) 417–425, <http://dx.doi.org/10.2514/1.A33636>.
- [6] D. Chipchark, Development of expulsion and orientation systems for advanced liquid rocket propulsion systems, Technical Report RTD-TDR-63-1048, USAF, 1963.
- [7] J. Martin, J. Holt, Magnetically Actuated Propellant Orientation Experiment, Controlling fluid Motion With Magnetic Fields in a Low-Gravity Environment, Technical Report TM-2000-210129, NASA, 2000.
- [8] S. Papell, Low viscosity magnetic fluid obtained by the colloidal suspension of magnetic particles, 1963, US Patent 3215572.
- [9] S. Kaneko, T. Ishiyama, T. Sawada, Effect of an applied magnetic field on sloshing pressure in a magnetic fluid, *J. Phys. Conf. Ser.* 412 (1) (2013) 012018, <http://dx.doi.org/10.1088/1742-6596/412/1/012018>.
- [10] M. Ohaba, S. Sudo, Liquid surface behavior of a magnetic liquid in a container subjected to magnetic field and vertical vibration, *J. Magn. Magn. Mater.* 149 (1995) 38–41, [http://dx.doi.org/10.1016/0304-8853\(95\)00332-0](http://dx.doi.org/10.1016/0304-8853(95)00332-0).
- [11] S. Sudo, H. Nishiyama, K. Katagiri, J. Tani, Interactions of magnetic field and the magnetic fluid surface, *J. Intell. Mater. Syst. Struct.* 10 (6) (1999) 498–504, <http://dx.doi.org/10.1106/N3PX-57EL-F43B-L4AO>.
- [12] T. Ishiyama, S. Kaneko, S. Takemoto, T. Sawada, Relation between dynamic pressure and displacement of free surface in two-layer sloshing between a magnetic fluid and silicone oil, *Mater. Sci. Forum* 792 (2014) 33–38, <http://dx.doi.org/10.4028/www.scientific.net/MSF.792.33>.
- [13] T. Sawada, Y. Ohira, H. Houda, Sloshing motion of a magnetic fluid in a cylindrical container due to horizontal oscillation, *Energy Convers. Manage.* 43 (3) (2002) 299–308, [http://dx.doi.org/10.1016/S0196-8904\(01\)00103-0](http://dx.doi.org/10.1016/S0196-8904(01)00103-0).
- [14] K. Ohno, M. Shimoda, T. Sawada, Optimal design of a tuned liquid damper using a magnetic fluid with one electromagnet, *J. Phys.: Condens. Matter* 20 (20) (2008) 204146, <http://dx.doi.org/10.1088/0953-8984/20/20/204146>.
- [15] K. Ohno, H. Suzuki, T. Sawada, Analysis of liquid sloshing of a tuned magnetic fluid damper for single and co-axial cylindrical containers, *J. Magn. Magn. Mater.* 323 (10) (2011) 1389–1393, <http://dx.doi.org/10.1016/j.jmmm.2010.11.052>.
- [16] F.T. Dodge, L.R. Garza, Free-surface vibrations of a magnetic liquid, *J. Eng. Ind.* 94 (1) (1972) 103–108, <http://dx.doi.org/10.1115/1.3428097>.
- [17] J. Hochstein, R. Warren Jr., George Schmidt Jr., Magnetically actuated propellant orientation (MAPO) experiment - pre-flight flow field predictions, in: 35th Aerospace Sciences Meeting and Exhibit, 1997, pp. 1–11, <http://dx.doi.org/10.2514/6.1997-570>.
- [18] J. Marchetta, J. Hochstein, Fluid capture by a permanent ring magnet in reduced gravity, in: Proceedings of the 37th Aerospace Sciences Meeting and Exhibit, Reno, NV, USA, American Institute of Aeronautics and Astronautics, 1999, pp. 1–14, <http://dx.doi.org/10.2514/6.1999-845>.
- [19] J. Marchetta, J. Hochstein, Simulation and dimensionless modeling of magnetically induced reorientation, in: Proceedings of the 38th Aerospace Sciences Meeting and Exhibit, Reno, NV, USA, American Institute of Aeronautics and Astronautics, 2000, pp. 1–13, <http://dx.doi.org/10.2514/6.2000-700>.
- [20] J. Marchetta, J. Hochstein, D. Sauter, B. Simmons, Modeling and prediction of magnetic storage and reorientation of LOX in reduced gravity, in: 40th AIAA Aerospace Sciences Meeting & Exhibit, American Institute of Aeronautics and Astronautics, 2002, pp. 1–19, <http://dx.doi.org/10.2514/6.2002-1005>.
- [21] J.G. Marchetta, Simulation of LOX reorientation using magnetic positive positioning, *Microgravity Sci. Technol.* 18 (1) (2006) 31, <http://dx.doi.org/10.1007/BF02908417>.

- [22] J. Marchetta, K. Roos, A three-dimensional computational simulation of magnetic positive positioning, in: 45th AIAA Aerospace Sciences Meeting and Exhibit, 2007, pp. 1–11, <http://dx.doi.org/10.2514/6.2007-956>.
- [23] J. Marchetta, K. Roos, Simulating magnetic positive positioning of liquids in a transient acceleration field, in: 46th AIAA Aerospace Sciences Meeting and Exhibit, 2008, pp. 1–11, <http://dx.doi.org/10.2514/6.2008-820>, AIAA Paper 2008-820.
- [24] J.G. Marchetta, B.D. Simmons, J.I. Hochstein, Magnetic retention of LO2 in an accelerating environment, *Acta Astronaut.* 62 (8) (2008) 478–490, <http://dx.doi.org/10.1016/j.actaastro.2008.01.016>.
- [25] J. Marchetta, A. Winter, Simulation of magnetic positive positioning for space based fluid management systems, *Math. Comput. Modelling* 51 (9) (2010) 1202–1212, <http://dx.doi.org/10.1016/j.mcm.2010.01.002>.
- [26] A. Romero-Calvo, T.H. Hermans, G.C. Gómez, L.P. Benítez, M.H. Gutiérrez, E. Castro-Hernández, Ferrofluid dynamics in microgravity conditions, in: Proceedings of the 2nd Symposium on Space Educational Activities, Budapest, Hungary, 2008, pp. 1–5.
- [27] A. Romero-Calvo, T.H. Hermans, L.P. Benítez, E. Castro-Hernández, Drop your thesis! 2017 experiment report - ferrofluids dynamics in microgravity conditions, European Space Agency - Erasmus Experiment Archive, 2018.
- [28] A. Romero-Calvo, G. Cano-Gómez, T.H. Hermans, L. Parrilla Benítez, M. Herrada, E. Castro-Hernández, Total magnetic force on a ferrofluid droplet in microgravity, *Exp. Therm Fluid Sci.* 117 (2020) 110124, <http://dx.doi.org/10.1016/j.expthermflusci.2020.110124>.
- [29] A. Romero-Calvo, A. García-Salcedo, F. Garrone, I. Rivoalen, G. Cano-Gómez, E. Castro-Hernández, M.H. Gutiérrez, F. Maggi, StELLIUM: A student experiment to investigate the sloshing of magnetic liquids in microgravity, *Acta Astronaut.* 173 (2020) 344–355, <http://dx.doi.org/10.1016/j.actaastro.2020.04.013>.
- [30] A. Romero-Calvo, G. Cano Gómez, E. Castro-Hernández, F. Maggi, Free and forced oscillations of magnetic liquids under low-gravity conditions, *J. Appl. Mech.* 87 (2) (2020) 021010, <http://dx.doi.org/10.1115/1.4045620>.
- [31] J.C. Boulware, H. Ban, S. Jensen, S. Wassom, Experimental studies of the pressures generated by a liquid oxygen slug in a magnetic field, *J. Magn. Magn. Mater.* 322 (13) (2010) 1752–1757, <http://dx.doi.org/10.1016/j.jmmm.2009.12.022>.
- [32] K. Kinefuchi, H. Kobayashi, Theoretical and experimental study of the active control of bubble point pressure using a magnetic field and its applications, *Phys. Fluids* 30 (6) (2018) 062101, <http://dx.doi.org/10.1063/1.5034222>.
- [33] A. Causevica, P. Sahli, F. Hild, K. Grunwald, M. Ehresmann, G. Herdrich, PAPELL: Interaction study of ferrofluid with electromagnets of an experiment on the international space station, in: Proceedings of the 69th International Astronautical Congress, 2018, pp. 1–5.
- [34] D. Ludovisi, S.S. Cha, N. Ramachandran, W.M. Worek, Heat transfer of thermocapillary convection in a two-layered fluid system under the influence of magnetic field, *Acta Astronaut.* 64 (11) (2009) 1066–1079, <http://dx.doi.org/10.1016/j.actaastro.2009.01.018>.
- [35] A. Bozhko, G. Putin, Thermomagnetic convection as a tool for heat and mass transfer control in nanosize materials under microgravity conditions, *Microgravity Sci. Technol.* 21 (1) (2009) 89–93, <http://dx.doi.org/10.1007/s12217-008-9059-7>.
- [36] B.A. Jackson, K.J. Terhune, L.B. King, Ionic liquid ferrofluid interface deformation and spray onset under electric and magnetic stresses, *Phys. Fluids* 29 (6) (2017) 064105, <http://dx.doi.org/10.1063/1.4985141>.
- [37] K. Lemmer, Propulsion for CubeSats, *Acta Astronaut.* 134 (2017) 231–243, <http://dx.doi.org/10.1016/j.actaastro.2017.01.048>.
- [38] R.E. Rosensweig, *Ferrohydrodynamics*, Dover Publications, 1997.
- [39] D.B. Kothe, R.C. Mjolsness, RIPPLE - A New model for incompressible flows with free surfaces, *AIAA J.* 30 (11) (1992) 2694–2700, <http://dx.doi.org/10.2514/3.11286>.
- [40] A. Myshkis, R. Wadhwa, *Low-Gravity Fluid Mechanics: Mathematical Theory of Capillary Phenomena*, Springer, 1987.
- [41] A. Romero-Calvo, M. Herrada, G. Cano-Gómez, H. Schaub, Advanced numerical simulation of magnetic liquid sloshing in microgravity, in: Proceedings of the International Astronautical Congress, the CyberSpace Edition, 2020, pp. 1–8.
- [42] H.M. Satterlee, W.C. Reynolds, *The Dynamics of Free Liquid Surface in Cylindrical Containers Under Strong Capillary and Weak Gravity Conditions*, Stanford University Mechanical Engineering Department, Report LG-2, 1964.
- [43] G. Yeh, Free and forced oscillations of a liquid in an axisymmetric tank at low-gravity environments, *J. Appl. Mech.* 34 (1) (1967) 23–28, <http://dx.doi.org/10.1115/1.3607644>.
- [44] E.A. Hulbert, R. Whitley, M.D. Klem, W. Johnson, L. Alexander, E. D'Aversa, J.-M. Ruault, C. Manfletti, International space exploration coordination group assessment of technology gaps for LOx/Methane propulsion systems for the global exploration roadmap, in: Proc. of the AIAA Space Forum 2016, 2016, pp. 1–17, <https://doi.org/10.2514/6.2016-5280>.
- [45] R.J. Meier, C.J. Schinkel, A. de Visser, Magnetisation of condensed oxygen under high pressures and in strong magnetic fields, *J. Phys. C: Solid State Phys.* 15 (5) (1982) 1015–1024, <http://dx.doi.org/10.1088/0022-3719/15/5/019>.
- [46] G.D. Grayson, M.L. Hand, E.C. Cady, Thermally coupled liquid oxygen and liquid methane storage vessel, 2009, US Patent 7, 568, 352 B2.
- [47] D.R. Lide, *CRC Handbook of Chemistry and Physics*, eighty fourth ed., CRC Press, 2003.
- [48] C. Wohlfarth, Surface tension of methane: Data sheet from Landolt-Börnstein - Group IV Physical Chemistry, Volume 24: “Supplement to IV/16”, 2008, http://dx.doi.org/10.1007/978-3-540-75508-1_20.
- [49] R.E. Rosensweig, Stress boundary-conditions in ferrohydrodynamics, *Ind. Eng. Chem. Res.* 46 (19) (2007) 6113–6117, <http://dx.doi.org/10.1021/ie060657e>.
- [50] M. Shliomis, Effective viscosity of magnetic suspensions, *Sov. Phys. JETP* 34 (1972) 1291–1294.
- [51] J. P. Shen, M. Doi, Effective viscosity of magnetic fluids, *J. Phys. Soc. Japan* 59 (1) (1990) 111–117, <http://dx.doi.org/10.1143/JPSJ.59.111>.
- [52] J.L. Neuringer, R.E. Rosensweig, Ferrohydrodynamics, *Phys. Fluids* 7 (12) (1964) 1927–1937, <http://dx.doi.org/10.1063/1.1711103>.
- [53] M. Utsumi, Mechanical models of low-gravity sloshing taking into account viscous damping, *J. Vib. Acoust.* 136 (1) (2013) <http://dx.doi.org/10.1115/1.4025439>.
- [54] B.M. Berkovsky, N.N. Smirnov, Capillary hydrodynamic effects in high magnetic fields, *J. Fluid Mech.* 187 (1988) 319–327, <http://dx.doi.org/10.1017/S0022112088000448>.
- [55] E. Mackor, A theoretical approach of the colloid-chemical stability of dispersions in hydrocarbons, *J. Colloid Sci.* 6 (5) (1951) 492–495, [http://dx.doi.org/10.1016/0095-8522\(51\)90019-0](http://dx.doi.org/10.1016/0095-8522(51)90019-0).
- [56] E.A. Elfimova, A.O. Ivanov, E.V. Lakhtina, A.F. Pshenichnikov, P.J. Camp, Sedimentation equilibria in polydisperse ferrofluids: critical comparisons between experiment, theory, and computer simulation, *Soft Matter* 12 (2016) 4103–4112, <http://dx.doi.org/10.1039/C6SM00304D>.
- [57] B. Luigjes, D.M.E. Thies-Weesie, A.P. Philipse, B.H. Erné, Sedimentation equilibria of ferrofluids: I. Analytical centrifugation in ultrathin glass capillaries, *J. Phys.: Condens. Matter* 24 (24) (2012) 245103, <http://dx.doi.org/10.1088/0953-8984/24/24/245103>.
- [58] J. Kurimský, M. Rajňák, P. Bartko, K. Paulovičová, R. Cimbala, D. Medved', M. Džamová, M. Timko, P. Kopčanský, Experimental study of AC breakdown strength in ferrofluid during thermal aging, *J. Magn. Magn. Mater.* 465 (2018) 136–142, <http://dx.doi.org/10.1016/j.jmmm.2018.05.083>.
- [59] P. Kopčanský, J. Černák, T. Tima, A. Zentko, M. Timko, P. Slančo, γ -Radiation induced sedimentation of magnetic particles in magnetic fluids, *J. Magn. Magn. Mater.* 85 (1) (1990) 103–106, [http://dx.doi.org/10.1016/0304-8853\(90\)90030-T](http://dx.doi.org/10.1016/0304-8853(90)90030-T).
- [60] V. Badescu, V. Craciun, G. Calugaru, The effect of irradiation on the properties of some ferrofluids used in hyperthermia, in: 2002 IEEE International Magnetism Conference (INTERMAG), 2002, p. FU7, <https://doi.org/10.1109/INTMAG.2002.1001376>.
- [61] M. Devi, N. Paul, D. Mohanta, A. Saha, Characteristic spectroscopic properties of γ -irradiated rare-earth oxide-based ferrofluids, *J. Exp. Nanosci.* 7 (5) (2012) 586–595, <http://dx.doi.org/10.1080/17458080.2010.548408>.
- [62] M. Devi, R. Das, D. Mohanta, K.K. Baruah, A. Saha, Enhanced magneto-optic activity of magnetite-based ferrofluids subjected to γ irradiation, *Appl. Phys. A* 106 (3) (2012) 757–763, <http://dx.doi.org/10.1007/s00339-011-6678-4>.
- [63] N. Tomašovičová, V. Závěšová, J. Kováč, M. Koneracká, M. Timko, I. Haysak, M. Koneracká, V. Zavisova, P. Kopčanský, I. Haysak, A. Okunev, A. Parlag, A. Fradkin, Radiation stability of biocompatible magnetic fluid, 2010.
- [64] N. Tomašovičová, I. Haysak, M. Koneracká, J. Kováč, M. Timko, V. Závěšová, A. Okunev, A. Parlag, A. Fradkin, V. Sakhno, P. Kopčanský, Magnetic properties of biocompatible magnetic fluid after electron irradiation, in: Proceedings of the European Conference Physics of Magnetism 2011 (PM-11), Poznaň, vol. 121, 2012, pp. 1302–1304, <https://doi.org/10.12693/APhysPolA.121.1302>.
- [65] N. Tomašovičová, I. Haysak, J. Kováč, M. Kubovčíková, V. Závěšová, M. Timko, A. Okunev, A. Zorkovská, P. Kopčanský, Radiation stability of the BSA modified biocompatible magnetic fluid, in: Proceedings of the 15th Czech and Slovak Conference on Magnetism, Košice, Slovakia, vol. 126, pp. 262–263, <https://doi.org/10.12693/APhysPolA.126.262>.
- [66] N. Simos, S. Fernandes, W. Mittig, F. Pellemoine, M. Avilov, M. Kostin, L. Mausner, R. Ronningen, M. Schein, G. Bollen, Performance degradation of ferrofluidic feedthroughs in a mixed irradiation field, *Nucl. Instrum. Methods Phys. Res. A* 841 (2017) 144–155, <http://dx.doi.org/10.1016/j.nima.2016.10.007>.
- [67] M. Pavlík, L. Kruželák, M. Mikita, M. Špes, S. Bucko, L. Lisoň, M. Kostelec, L. Beňa, P. Liptai, The impact of electromagnetic radiation on the degradation of magnetic ferrofluids, *Arch. Electr. Eng.* 66 (No 2 June) (2017) <http://dx.doi.org/10.1515/ae-2017-0027>.
- [68] S. Bhattacharya, K. Jenamoni, S. Nayar, Stability of biomimetic ferrofluids established by a systematic study using microwave irradiation at defined wattages, *J. Magn. Magn. Mater.* 324 (20) (2012) 3261–3266, <http://dx.doi.org/10.1016/j.jmmm.2012.05.001>.
- [69] P.R. Choudhury, Slurry fuels, *Prog. Energy Combust. Sci.* 18 (5) (1992) 409–427, [http://dx.doi.org/10.1016/0360-1285\(92\)90008-O](http://dx.doi.org/10.1016/0360-1285(92)90008-O).
- [70] B. Balaszewsky, J. Zakany, Metallized gelled propellants: Oxygen/RP-1/aluminum rocket combustion experiments, in: 31st Joint Propulsion Conference and Exhibit, San Diego, CA; United States, 1995, pp. 1–32, AIAA Paper 95-2435, <https://doi.org/10.2514/6.1995-2435>.

- [71] K.P. Doyle, M.A. Peck, Water electrolysis propulsion as a case study in resource-based spacecraft architecture (February 2020), IEEE Aerosp. Electron. Syst. Mag. 34 (9) (2019) 4–19, <http://dx.doi.org/10.1109/MAES.2019.2923312>.
- [72] P. Stelmachowski, A. Kopacz, P. Legutko, P. Indyka, M. Wojtasik, L. Ziemiański, G. Żak, Z. Sojka, A. Kotarba, The role of crystallite size of iron oxide catalyst for soot combustion, Catal. Today 257 (2015) 111–116, <http://dx.doi.org/10.1016/j.cattod.2015.02.018>, Air and Water Pollution Abatement Catalysis (AWPAC 2014).
- [73] D. Ghosh, A.K. Roy, A. Ghosh, Reduction of ferric oxide pellets with methane, Trans. Iron Steel Inst. Japan 26 (3) (1986) 186–193, <http://dx.doi.org/10.2355/isijinternational1966.26.186>.
- [74] E.R. Monazam, R.W. Breault, R. Siriwardane, G. Richards, S. Carpenter, Kinetics of the reduction of hematite (Fe₂O₃) by methane (CH₄) during chemical looping combustion: A global mechanism, Chem. Eng. J. 232 (2013) 478–487, <http://dx.doi.org/10.1016/j.cej.2013.07.091>.
- [75] F. Maggi, S. Dossi, C. Paravan, L. Galfetti, R. Rota, S. Cianfanelli, G. Marra, Iron oxide as solid propellant catalyst: A detailed characterization, Acta Astronaut. 158 (2019) 416–424, <http://dx.doi.org/10.1016/j.actaastro.2018.07.037>.
- [76] S. Gordon, B. McBride, Computer program for calculation of complex chemical equilibrium compositions and applications, 1994, NASA Reference Publication RP-1311.
- [77] I. Glassman, R. Sawyer, The Performance of Chemical Propellants, AGARDograph; no. 129, Technivision Services, Slough, England, 1970.
- [78] G. Sutton, O. Biblarz, Rocket Propulsion Elements, seventh ed., John Wiley & Sons, 2007.
- [79] A. Romero-Calvo, M.A. Herrada, T.H. Hermans, L. P. Benítez, G. Cano-Gómez, E. Castro-Hernández, Axisymmetric ferrofluid oscillations in a cylindrical tank in microgravity, Microgravity Sci. Technol. (2021) (accepted for publication).